Nuclear Engineering and Design 289 (2015) 60–72

Contents lists available at ScienceDirect

Nuclear Engineering and Design

journal homepage: www.elsevier.com/locate/nucengdes

RANS modeling for particle transport and deposition in turbulent duct flows: Near wall model uncertainties

S.T. Jayaraju[a,*], P. Sathiah[a], F. Roelofs[a], A. Dehbi[b]

[a] Nuclear Research and Consultancy Group (NRG), 1755ZG Petten, The Netherlands
[b] Paul Scherrer Institute (PSI), 5232 Villigen PSI, Switzerland

HIGHLIGHTS

- Near-wall modeling uncertainties in the RANS particle transport and deposition are addressed in a turbulent duct flow.
- Discrete Random Walk (DRW) model and Continuous Random Walk (CRW) model performances are tested.
- Several near-wall anisotropic model accuracy is assessed.
- Numerous sensitivity studies are performed to recommend a robust, well-validated near-wall model for accurate particle deposition predictions.

ARTICLE INFO

Article history:
Received 21 March 2014
Received in revised form 5 December 2014
Accepted 6 April 2015

ABSTRACT

Dust accumulation in the primary system of a (V)HTR is identified as one of the foremost concerns during a potential accident. Several numerical efforts have focused on the use of RANS methodology to better understand the complex phenomena of fluid–particle interaction at various flow conditions. In the present work, several uncertainties relating to the near-wall modeling of particle transport and deposition are addressed for the RANS approach. The validation analyses are performed in a fully developed turbulent duct flow setup. A standard $k-\varepsilon$ turbulence model with enhanced wall treatment is used for modeling the turbulence. For the Lagrangian phase, the performance of a continuous random walk (CRW) model and a discrete random walk (DRW) model for the particle transport and deposition are assessed. For wall bounded flows, it is generally seen that accounting for near wall anisotropy is important to accurately predict particle deposition. The various near-wall correlations available in the literature are either derived from the DNS data or from the experimental data. A thorough investigation into various near-wall correlations and their applicability for accurate particle deposition predictions are assessed. The main outcome of the present work is a well validated turbulence model with optimal near-wall modeling which provides realistic particle deposition predictions.

1. Introduction

A very high temperature or high temperature gas cooled reactor (HTGR) is under consideration as a fourth generation advanced nuclear reactor (CEA, 2006). The reactor uses graphite as a moderator and helium gas as a coolant. Because of high core outlet temperature, high thermal efficiency is achieved in these types of reactors. Moreover, there is no need for active safety systems to cool the reactor core as it is designed to lose heat by itself from natural circulation. A number of experimental and prototype reactors have been built and operated in the past. Examples of high temperature reactors are the Dragon reactor (United Kingdom), the Peach Bottom reactor (United States of America), AVR and THTR 300 (Germany) and the reactor at Fort St. Vrain (United States of America). At present, there are experimental reactors under operation in Japan and China (HTR-10). Apart from this, two full scaled HTGRs, the two-module plat HTR-PM, are under construction in China.

In a typical pebble bed reactor, the reactor core is made up of several hundred thousands of randomly stacked pebbles. These pebbles are primarily made of graphite and contain uranium dispersed in sand-size grains throughout the pebble. One of the main sources of dust production is due to the abrasion of randomly stacked graphite pebbles. The generated dust is essentially composed of carbonaceous compounds, fission and activation products. In a 400 MW thermal pebble-bed HTR, abraded dust is anticipated to be in the range of 30–100 kg/yr (Kissane et al., 2011). Various

* Corresponding author. Tel.: +31 224 56 8140; fax: +31 224 56 8490.
E-mail address: jayaraju@nrg.eu (S.T. Jayaraju).

http://dx.doi.org/10.1016/j.nucengdes.2015.04.011
0029-5493/

Nomenclature

Roman symbols

$\bar{u}$	time-averaged mean velocity components computed from a RANS simulation in streamwise direction
$\bar{v}$	time-averaged mean velocity components computed from a RANS simulation in wall-normalc direction
$\bar{w}$	time-averaged mean velocity components computed from a RANS simulation in spanwise direction
$\vec{u_p}$	particle velocity vector
$\vec{u}$	fluid velocity vector
$\vec{x_p}$	particle position
$\vec{f}$	body forces and the surface forces acting on the particle
$\vec{f}_{brownian}$	Brownian force acting on the particle
$\vec{f}_{drag}$	drag force acting on the particle
$\vec{f}_{gravity}$	gravity force acting on the particle
$\vec{f}_{lift}$	lift force acting on the particle
C_0	constant value of 14
C_c	Cunnigham slip correction factor
C_d	drag coefficient
d_p	particle diameter
f_i	near-wall functions, for $i = u, v, z$
g_x	gravitational acceleration in x direction
J	particle mass flux to the wall per unit time
k	turbulent kinetic energy
l_e	eddy length scale
N_0	initial number of particles uniformly distributed in a region within a distance y_0^+
N_d	number of deposited particle in the time duration t_d^+
Re_p	particle Reynolds number
S	spectral intensity
Stk	Stokes number
T	temperature
t	time
t_c	crossing time
t_d^+	non dimensional time duration of deposition
t_e	eddy time scale
u'	fluid fluctuating velocity component in streamwise direction
u_τ	friction velocity
u_d^+	non-dimensional deposition velocity
u_f	fluid velocity magnitude
u_p	particle velocity magnitude
u_{rms}	RMS of velocity component in streamwise direction
v'	fluid fluctuating velocity component in wall-normalc direction
v_{rms}	RMS of velocity component in wall-normal direction
w'	fluid fluctuating velocity component in spanwise direction
w_{rms}	RMS of velocity component in spanwise direction
x	coordinate in x direction
y	coordinate in y direction
y^+	non-dimensional wall distance
y_0^+	non-dimensional wall distance of first cell at the wall
z	coordinate in z direction

Greek symbols

ϵ	turbulent dissipation rate
κ_B	Boltzmann constant
λ	gas molecular mean free path
μ	dynamic viscosity
ν	kinematic viscosity
ρ	fluid density
ρ_p	particle density
τ_L^+	normalized Lagrangian time scale
τ_L	Lagrangian time scale
τ_p	particle relaxation time
τ_w	wall shear stress
ξ_i	Gaussian random number with zero mean and variance dt along the $i = x, y, z$ directions
ζ	random number drawn from a normal probability distribution with zero mean and unit standard deviation.

Subscripts and superscripts

$'$	fluctuating quantities
$-$	Reynolds averaged mean quantities
$^+$	normalized quantity

Acronyms

CFD	Computational Fluid Dynamics
DNS	Direct Numerical Simulation
LES	Large Eddy Simulation
RANS	Reynolds Average Navier Stokes equations
HTR	High Temperature Reactor
HTGR	High Temperature Gas Cooled Reactor
CRW	Continuous Random Walk model
DRW	Discrete Random Walk model
CFWN	Continuous Filtered White-Noise model
EIM	Eddy Interaction Model
RMS	Root Mean Square value
SIMPLE	Semi-Implicit Method for Pressure-Linked Equations

sizes of the dust particles are reported in the literature. For example, dust particle size measured at the end of the life cycle of the pebble-bed AVR reactor was found to be largely submicron with a geometric-mean diameter of 0.6 μm (Gottaut and Kruger, 1990). Recent experiments for HTR-10 indicate a geometric-mean diameter of about 2.2 μm (Luo et al., 2005). The dust produced due to abrasion is eventually carried by helium gas to the primary circuit and gets deposited in its main components such as the main pipes systems, the heat exchangers (steam generators, intermediate heat exchangers or recuperators) and turbo-machinery if applicable. The dust transport, deposition and re-suspension in the primary system of these reactors is identified as one of the foremost concerns during a potential accident (Kissane, 2009). The present paper is focused on the accurate prediction of dust transport and deposition which is an important step in the design of these types of reactors.

Computational-Fluid-Dynamics (CFD) modeling has emerged as a useful tool in simulating the particle transport and deposition phenomena. While Direct-Numerical-Simulation (DNS) and Large-Eddy-Simulation (LES) are the advanced modeling methodologies which result in realistic particle deposition predictions, they are computationally very expensive for real plant applications. The widely used Reynolds-Averaged-Navier-Stokes (RANS) methodology is the most practical approach to consider. Within the RANS modeling of particle transport and deposition, several approaches

are available in the literature to model the effects of the flow turbulence on the particle motion, namely the discrete random walk (DRW), continuous filtered white-noise (CFWN) model and continuous random walk (CRW). One of the most frequently used models in commercial CFD codes is the DRW (Gosman and Ioannides, 1981). Some authors in the literature also use the term eddy interaction model (EIM) to describe this type of model. EIM was first introduced by Gosman and Ioannides (1981) with the assumption of isotropic turbulence in the complete domain. Within this approach, the effects of turbulence on the particles are modeled as a succession of interaction between particles and eddies. These eddies have a finite lifetime and size and are characterized by a random velocity fluctuation, which obeys a Gaussian distribution. The DRW approach has been successfully applied to study particle transport and deposition in various flow configurations (Kallio and Reeks, 1989; Wang and James, 1999; Matida et al., 2004; Lai and Chen, 2006; Tian and Ahmadi, 2007). The CFWN model was proposed by He and Ahmadi (1999) in which the instantaneous fluid velocity is simulated using the Langevin equation for a given local mean velocity and local velocity fluctuation. The model treats the instantaneous velocities in a continuous way, and the particles are tracked through this continuous instantaneous field. CRW is another class of models, which solves the normalized Langevin equation (Dehbi, 2009, 2008b, 2010; Dehbi and de Crcy, 2011). The model has been successfully applied to simulate particle deposition in inhomogeneous flow configurations such as mixing layer (Maciines and Bracco, 1992) and shear flows (Bockell and Loth, 2006). The first main objective of the present work is to assess the performance of the DRW approach as opposed to the CRW approach.

For wall bounded flows, it is generally seen that accounting for near wall anisotropy is important to predict accurate particle deposition (Gosman and Ioannides, 1983). Most of the recent literature on particle deposition using RANS modeling of wall bounded flows focusses on accurate modeling of the near-wall anisotropy. In the work of Kallio and Reeks (1989), the turbulent RMS velocity profiles obtained from the experimental data are used to account for anisotropy in the near-wall turbulence. CFD simulations are performed for particle deposition in a pipe at different particle relaxation times and different particle fluid density ratios. The simulation results agreed well with experimental measured deposition velocities. Wang and James (1999) accounted for anisotropic effects of turbulence by using three functions to specify the local velocity fluctuations close to the wall. The results of particle deposition agreed well with the experimental data of Liu and Agarwal (1974). Matida et al. (2004) proposed near wall correction of the turbulent kinetic energy in the EIM model to simulate particle deposition in an idealized mouth-throat geometry. The simulation results show relatively good agreement with the experimental data, when the near wall corrections are considered. Lai and Chen (2006) used a correction for near wall turbulent kinetic energy to account for near-wall anisotropy. The model was used to study the particle transport and deposition in a room. The trends of model prediction were in good agreement with empirical correlations. Tian and Ahmadi (2007) performed calculations to study the transport and deposition of nano and micro-particles in a turbulent duct by using corrections for the near-wall quadratic variation of the wall-normal turbulent fluctuation. They concluded that the accurate prediction of particle deposition rates is obtained by considering anisotropic near-wall modeling. Dehbi (2008a) used velocity fluctuations obtained from DNS data of fully developed duct flow which were fitted into functions, and used in the near wall region to account for the flow anisotropy. The proposed approach is tested against particle deposition in a turbulent pipe flow and flow in a 90° pipe bend. It was concluded that the results are in a better match with the experimental data in comparison to the isotropic model. Agnihotri et al. (2012) have studied the deposition of mono-disperse aerosols on a simplified human upper airway model using the so-called helicity-EIM which adopts new correction functions for eddy interaction model. These correlation functions are formulated in such a way that it does not require the estimation of y+ for each case in an attempt to improve the accuracy of predicting aerosol deposition. The results of the helicity-EIM model were of similar accuracy compared to those of Wang and James (1999). Recently, Lecrivain et al. (2014) have studied multi-layer deposition in an obstructed channel flow using a variant of anisotropic CRW model. The numerical results were in good accordance with the on-site wind tunnel experiments.

From the above results, it is clear that accounting for near-wall anisotropy improves the particle deposition predictions. The various near-wall correlations used in the literature are either derived from the DNS data or from the experimental data. Regarding the near-wall anisotropy modeling, there are several uncertainties which need to be addressed such as: Which model is most accurate?; Is the DNS data near-wall Reynolds number dependent?; Is the DNS data near-wall cross-section specific?; Different authors use different y^+ cut-off values below which anisotropy is considered. Which y^+ cut-off should be used?; In the viscous sub-layer (y^+<5), different values of Lagrangian time scales are used in the literature. Which value of Lagrangian time scale yields best results?. The main objective of this paper is to answer all these uncertainties in a systematic way. By doing so, one would be able to define a robustly validated RANS model which can be used for particle transport and deposition predictions.

2. Particle governing equations

The following assumptions are invoked for the particle phase:

- The particle is taken to be spherical.
- The ratio of the particle to the fluid density is assumed to very large.
- Air flow is not affected by the presence of particles and effects of the particle on turbulence are neglected i.e. one way coupling is assumed.
- The particle phase is dilute i.e. the volume loading of the particles is assumed to be negligibly small.
- Particle-particle interactions are neglected. The particle rotational and thermophoretic forces are assumed to be zero.

Taking the above assumptions into consideration, the Lagrangian equations governing the particle motion following Crowe et al. (1998) are written as:

$$\frac{d\vec{x}_p}{dt} = \vec{u}_p \tag{1}$$

and

$$\frac{d\vec{u}_p}{dt} = \vec{f} \tag{2}$$

where, $\vec{x}_p$ is the particle position, and $\vec{u}_p$ is the velocity of the particle. $\vec{f}$ represents all the body forces and the surface forces acting on the particle. Example of body force acting on the mass of the particle is gravity, while the surface forces are due to drag, which represents a momentum coupling between the two phases (Sommerfeld et al., 1992). The forces, which are relevant for the present work, are the the drag, gravity and Brownian diffusion which are described below:

$$\vec{f} = \vec{f}_{drag} + \vec{f}_{gravity} + \vec{f}_{lift} + \vec{f}_{brownian} \tag{3}$$

2.1. Drag force

Generally, the particle moves with a different velocity than the fluid at any given point. The difference in fluid velocity ($\vec{u}$) and the particle velocity ($\vec{u}_p$), is termed as the *slip velocity* ($\vec{u} - \vec{u}_p$), which leads to an unbalanced pressure distribution as well as viscous stresses on the particle surface. This yields a resulting force called a *drag force*. For a rigid sphere, the drag force for unit particle mass is given by $\vec{f}_{drag}(\vec{u} - \vec{u}_p)$. $\vec{f}_{drag}$ is defined as (Sommerfeld et al., 1992):

$$\vec{f}_{drag} = \frac{1}{\tau_p}\frac{C_d Re_p}{24}. \tag{4}$$

Here, the drag coefficient C_d is a function of particle Reynolds number, Re_p. Various experimental based empirical correlations for the drag coefficient as a function of Re_p are available in the literature (Sommerfeld et al., 1992). The Reynolds number Re_p of the particle is defined as:

$$Re_p = \rho\, d_p \frac{|\vec{u} - \vec{u}_p|}{\mu}. \tag{5}$$

The term τ_p in Eq. (4) is the particle relaxation time which is defined as:

$$\tau_p = \frac{C_c \rho_p d_p^2}{18\mu} \quad \text{for} \quad Re_p \le 1 \tag{6}$$

$$\tau_p = \frac{4}{3}\frac{\rho_p}{\rho}\frac{C_c d_p^2}{C_d|\vec{u} - \vec{u}_p|} \quad \text{for} \quad Re_p > 1 \tag{7}$$

where, d_p is the particle diameter, ρ_p is the particle density and C_c is the Cunnigham slip correction factor given by:

$$C_c = 1 + \frac{2\lambda}{d_p}(1.257 + 0.4e^{(1.1 d_p/2\lambda)}) \tag{8}$$

where, λ is the gas molecular mean free path.

2.2. Gravity force

A particle when subjected to a gravitational field experiences a force in the direction of the gravitational acceleration. The particle also experiences a buoyancy force opposite to the direction of gravity. This force is equal to the weight of the displaced fluid according to Archimedes principle. The net force due to gravity is given by:

$$\vec{f}_{gravity} = g_x \frac{(\rho_p - \rho)}{\rho_p} \tag{9}$$

where, g_x is the gravitational acceleration in x direction, ρ and ρ_p are the density of the fluid and the particle, respectively.

2.3. Lift force

A particle entrained in a shear flow field may experience a shear induced lift force perpendicular to the main flow direction. Lift force becomes important close to the walls as the fluid velocity gradients as well as the difference between particle and fluid velocity are the largest here.

The Saffman lift force is modeled as (Li and Ahmadi, 1992):

$$\vec{f}_{saffman} = \frac{5.188\nu^{0.5}\rho_f d_{ij}}{\rho_p d_p (d_{lk} d_{kl})^{0.25}}(\vec{u} - \vec{u}_p) \tag{10}$$

This formulation is mainly intended for small particle Reynolds numbers and typically sub-micron particles.

2.4. Brownian diffusion

Any given fluid at the molecular level is associated with random molecular movements and collisions. When the particle response time becomes less than the time required for the molecular impacts in a fluid, the particles have enough time to respond to these molecular changes in the fluid. Brownian diffusion is characterized by random motion of particles where the particles generally tend to move from higher particle concentration region towards the lower particle concentration region.

The Brownian force components are modeled as (Li and Ahmadi, 1992):

$$\vec{f}_b = \xi_i \sqrt{\frac{\pi S}{\Delta t}} \tag{11}$$

where, ξ_i is a Gaussian random number with zero mean and unit variance. S is the spectral intensity given by:

$$S = \frac{216\rho\nu k_B T}{\pi\rho {d_p}^5 {\rho_p}^2 C_c}. \tag{12}$$

Here, k_B is the Boltzmann constant and T is the temperature. This formulation of Brownian diffusion is important for submicron particles.

3. Deposition Regimes

Deposition mechanisms can be best understood by taking an example of deposition in a smooth pipe flow. Fig. 1 shows the typical characteristic regimes of dimensionless deposition velocity as a function of dimensionless particle relaxation time τ^+. As shown in the figure, the most common classification of deposition is divided into three distinct regimes. If τ^+ ($Stk_{near-wall}$) is smaller than about 0.25, the particles are small enough to respond to the changes in the near-wall turbulent flow motions. As a result, Brownian motion becomes an important mechanism for the particle deposition. This regime is indicated as the diffusional deposition regime. If τ^+ is bigger than about 20, then the particles have practically no time to respond to the changes in the near-wall flow motions. Instead, their motion might only be affected by the larger eddies in the bulk of the flow. Consequently, these large particles deposit on the walls through momentum given to them by the large eddies. This regime is indicated as the inertia-impaction regime. If τ^+ is in the approximate range between 0.25 and 20, the particles are expected to only partly follow the near-wall eddies. Such particles either shoot ahead or lag behind the near-wall eddies. Hence, these particles may get deposited either due to Brownian motion or by impaction. This regime is indicated a the diffusion-impaction regime.

4. Particle transport models

The present section describes the two particle transport models studied in the present work, namely the Discrete Random Walk model and the Continuous Random Walk model. The conceptual difference between these two models is in terms of how the flow fluctuations are seen by the particles. As the name suggests, the fluid flow fluctuations are modeled in a more realistic and continuous way in CRW model, as opposed to a more filtered/discrete approach taken by the DRW model (Macinnes and Bracco, 1992).

4.1. Discrete Random Walk model

One of the most frequently used models is the eddy interaction model (EIM) first introduced by Hutchinson et al. (1971) and further developed by Gosman and Ioannides (1981). The EIM is also referred to as the Discrete-Random-Walk (DRW) model.

The instantaneous fluid velocity is represented as the sum of the mean and fluctuating velocity as follows:

$$u = \bar{u} + u' \tag{13}$$

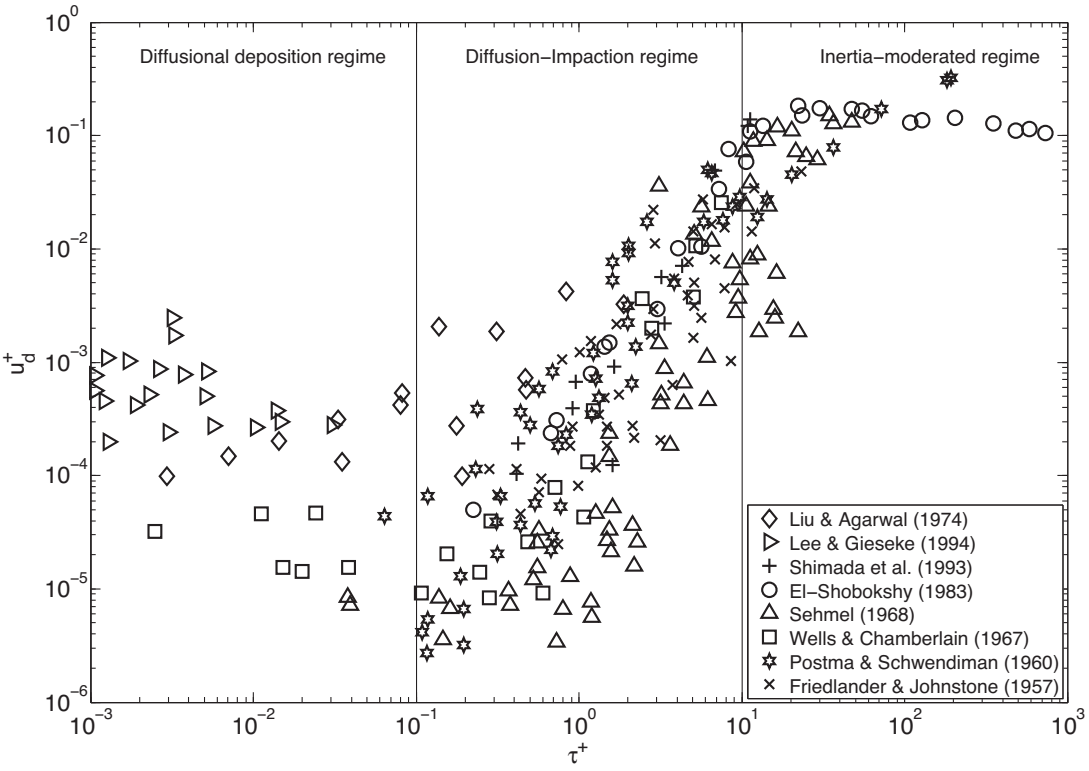

Fig. 1. Characteristic regimes of dimensionless deposition velocity as a function of dimensionless particle relaxation time.

$$v = \bar{v} + v' \tag{14}$$

$$w = \bar{w} + w' \tag{15}$$

where $\bar{u}$, $\bar{v}$ and $\bar{w}$ are the time-averaged mean velocity components computed from a RANS simulation. u', v' and w' are the fluid fluctuating velocities defined as $\sqrt{\bar{u'^2}}$, $\sqrt{\bar{v'^2}}$ and $\sqrt{\bar{w'^2}}$. In most commercial CFD solvers, the fluid fluctuating velocity components are modeled assuming isotropic turbulence.

The chosen fluctuation is referred to a turbulent eddy whose size (length scale) and life-time(time scale) is known. Sommerfeld et al. (1992) proposed the following relations for the eddy parameters:

$$t_e = 2\tau_L = c_t \frac{k}{\varepsilon} \tag{16}$$

and

$$l_e = t_e \sqrt{\frac{2}{3}k} \tag{17}$$

where, c_t is an empirical constant set to 0.3, t_e is the eddy time scale, l_e is the eddy length scale and τ_L is the Lagrangian time scale. It represents the time over which the velocity of a particle is self-correlated.

It is accepted that the fluctuation remains constant within a turbulent eddy for a certain interaction time, while the respective mean velocity component (U) is varied according to particle position. The interaction time is the minimum of two time scales, one being the turbulent eddy lifetime and the other is the crossing-time of the particle located within the eddy (Gosman and Ioannides, 1981).

$$t_{\text{int}} = \min(t_e, t_c) \tag{18}$$

The crossing-time is defined as

$$t_c = -\tau_p \ln\left[1 - \left(\frac{l_e}{\tau_p|\vec{u} - \vec{u}_p|}\right)\right] \tag{19}$$

where τ_p is the particle relaxation time, l_e the eddy length scale and $|\vec{u} - \vec{u}_p|$ the magnitude of slip velocity.

In circumstances where $l_e/(\tau_p|\vec{u} - \vec{u}_p|) > 1$, Eq. (19) has no solution. This can be interpreted as the particle trapped by an eddy, in which case $t_{int} = t_e$ (Gosman and Ioannides, 1981). This procedure may be repeated for as many interaction times as required for the particle to traverse the required distance. If a statistically significant number of particles are tracked in this way, the ensemble averaged behavior should represent the turbulent dispersion induced by the prevailing fluid field (Gosman and Ioannides, 1981).

The Eulerian statistics of fluid fluctuating velocities u', v' and w' appearing in Eqs. (13)–(15) needs to be specified. In most of the state-of-the-art commercial CFD solvers, the fluid fluctuating velocities are specified assuming isotropic turbulence. Most stochastic isotropic models in practical use are derived from Gosman and Ioannides (1981) which is given by:

$$u' = v' = w' = \sqrt{\frac{2}{3}k} * \zeta \quad [m/s] \tag{20}$$

where k is the turbulent kinetic energy which may be determined from any typical two-equation turbulence closure model such as the $k-\varepsilon$ model or the $k-\omega$ model. ζ is a random number drawn from a normal probability distribution with zero mean and unit standard deviation.

In the present paper, the near-wall correlation of Dreeben and Pope (1997) coupled with the DRW model is evaluated.

4.2. Continuous Random Walk model

Recently, Dehbi (2008a,b, 2009, 2010) presented in detail a CRW model for the prediction of particle deposition in wall bounded flows. The main equations used in the modeling are presented here. Within this approach, the particle deposition modeling is divided into two regions namely, the boundary layer region with strong anisotropic turbulence and bulk flow region with isotropic

turbulence. The model is based on a Langevin equation. The Langevin equation takes different forms depending on the particle location which could be in the boundary layer or in the bulk region. In the **boundary layer region**, the normalized Langevin equation for streamwise, wall-normal and spanwise directions are given by:

$$d\left(\frac{u'}{u_{rms}}\right) = -\left(\frac{u'}{u_{rms}}\right).\frac{\Delta t}{\tau_L} + \sqrt{\frac{2}{\tau_L}}.d\xi_x \tag{21}$$

$$d\left(\frac{v'}{v_{rms}}\right) = -\left(\frac{v'}{v_{rms}}\right).\frac{\Delta t}{\tau_L} + \sqrt{\frac{2}{\tau_L}}.d\xi_y + \frac{\partial v_{rms}}{\partial y}.\frac{\Delta t}{1+Stk} \tag{22}$$

$$d\left(\frac{w'}{w_{rms}}\right) = -\left(\frac{w'}{w_{rms}}\right).\frac{\Delta t}{\tau_L} + \sqrt{\frac{2}{\tau_L}}.d\xi_z \tag{23}$$

where, u', v' and w' are the fluid fluctuating velocity components in streamwise, wall-normal and spanwise directions. u_{rms}, v_{rms} and w_{rms} are the corresponding RMS velocity components. x, y and z are the coordinates in x, y and z directions. ξ_x, ξ_y and ξ_z are the Gaussian random numbers with zero mean and variance dt.

In the above equation, Stk is a particle Stokes number, which is the ratio of particle relaxation time to the Lagrangian time scale and is given by:

$$Stk = \frac{\tau_p}{\tau_L}. \tag{24}$$

The last term on the right hand side of Eq. (22) is the mean drift correction term, which is added to avoid the un-physical migration of small inertial particles towards the boundary layer. Lecrivain and Hampel (2012) indicated that neglecting this term leads to overestimation of the particle deposition.

In the **bulk flow region**, the following equations for the normalized Langevin equations are solved for streamwise, wall-normal and spanwise directions:

$$d\left(\frac{u'}{u_{rms}}\right) = -\left(\frac{u'}{u_{rms}}\right).\frac{\Delta t}{\tau_L} + \sqrt{\frac{2}{\tau_L}}.d\xi_x + \frac{1}{3u_{rms}}.\frac{\partial k}{\partial x}.\frac{dt}{1+Stk} \tag{25}$$

$$d\left(\frac{v'}{v_{rms}}\right) = -\left(\frac{v'}{v_{rms}}\right).\frac{\Delta t}{\tau_L} + \sqrt{\frac{2}{\tau_L}}.d\xi_y + \frac{1}{3v_{rms}}.\frac{\partial k}{\partial y}.\frac{dt}{1+Stk} \tag{26}$$

$$d\left(\frac{w'}{w_{rms}}\right) = -\left(\frac{w'}{w_{rms}}\right).\frac{\Delta t}{\tau_L} + \sqrt{\frac{2}{\tau_L}}.d\xi_z + \frac{1}{3w_{rms}}.\frac{\partial k}{\partial z}.\frac{dt}{1+Stk} \tag{27}$$

where, k is the turbulent kinetic energy.

The fluid fluctuating velocities are defined from the Langevin equations. Depending on the region of interest, two sets of Langevin equations are solved. In the bulk flow region, Eqs. (25)–(27) are solved to obtain the fluid fluctuating velocities u', v' and w'. Assuming isotropic turbulence in the bulk fluid flow, the RMS velocities in Eqs. (25)–(27) are given by:

$$u_{rms} = v_{rms} = w_{rms} = \sqrt{\frac{2}{3}k} \tag{28}$$

where, k is the turbulent kinetic energy.

In the near-wall region, Eqs. (21)–(23) are solved to obtain the fluid fluctuating velocities u', v' and w'. The RMS velocities in these equations needs to be prescribed based on anisotropic near-wall behavior of the RMS velocities. There are several correlations proposed in the literature to model the the near-wall anisotropy. These correlations are discussed in detail in Section 5.

To close the Langevin equations, the Lagrangian time scale τ_L must be specified. There are several correlations available for the Lagrangian time-scales are discussed in the work of Lecrivain and Hampel (2012). In the present work, the Lagrangian time scale correlation approximated by the fits provided by Kallio and Reeks (1989) is used. In the boundary layer, the Lagrangian time scale is given as follows:

$$\tau_L^+ \simeq 10 \quad \text{for} \quad y^+ < 5 \tag{29}$$

$$\tau_L^+ = 7.122 + 0.5731y^+ - 0.00129y^{+2} \quad \text{for} \quad 5 < y^+ < 200 \tag{30}$$

where, τ_L^+ is defined as:

$$\tau_L^+ = \frac{\tau_L u^{*2}}{\nu} \tag{31}$$

Here, y^+ is the normalized wall distance, which is given by:

$$y^+ = \frac{yu^*}{\nu} \tag{32}$$

The friction velocity u^* is given by:

$$u^* = \sqrt{\frac{\tau_w}{\rho}} \tag{33}$$

where, τ_w is the wall shear stress.

In the bulk flow, the Lagrangian time scale is given by:

$$\tau_L = \frac{2}{C_o}\frac{k}{\varepsilon} \tag{34}$$

where, C_o is constant with a value of 14 (Mito and Hanratty, 2004, 2002).

5. Near-wall model uncertainties

5.1. Correlations for RMS velocities

In many applications, turbulence can be approximated as being isotropic in the bulk region when high swirls and rapid changes in the strain rate are not present. However, in the near-wall region, the turbulent velocity fluctuations are certainly strongly anisotropic. In fact, the RMS of the wall-normal component of velocity in a channel flow can be orders of magnitude smaller than the streamwise or the spanwise component (Marchioli et al., 2008). In order to take this near wall anisotropy into account, there are several near-wall modifications proposed in the literature. These correlations are based on channel flows. The relevant modifications are summarized in this section.

5.1.1. Tian and Ahmadi

Based on the experimental measurements and the DNS data of Kim et al. (1987) and Ounis et al. (1993), it is well-known that continuity requires the wall-normal RMS turbulence velocity fluctuation to follow a quadratic variation. Tian and Ahmadi (2007) proposed the following correlation:

$$v_{rms} = Ay^{+2} \quad \text{for} \quad y^+ < 4 \tag{35}$$

where, $v_{rms} = \sqrt{\overline{v'^2}}/u^*$. A value of A is suggested to be 0.008 using the DNS data of Ounis et al. (1993).

5.1.2. Kallio and Reeks

Based on several experimental data, Kallio and Reeks (1989) proposed to use the following near-wall correction to the wall-normal velocity fluctuation:

$$v_{rms} = \frac{0.005y^{+2}}{1 + 0.002923y^{+2.128}} \tag{36}$$

It was indicated that these correlations are valid in the near wall region where y^+<200.

5.1.3. Matida et al.

Considering that the wall normal fluctuating component plays a major role in the particle deposition, Matida et al. (2004) suggested to apply the wall-normal function proposed by Wang and James (1999) for all three fluctuating components as follows:

$$u_{rms} = v_{rms} = w_{rms} = [1 - \exp(-0.02y^+)]\sqrt{\frac{2k}{3}} \tag{37}$$

The above formulation was applied for different y^+ ranges based on the flow-rate.

5.1.4. Wang and James

Wang and James (1999) introduced three functions f_u, f_v and f_w to specify the local RMS velocities close to the wall. These functions are derived from the DNS data of a duct flow (Kim et al., 1987; Mansour et al., 1988). The RMS velocities were defined as:

$$u_{rms} = f_u\zeta\sqrt{\frac{2k}{3}} \tag{38}$$

$$v_{rms} = f_v\zeta\sqrt{\frac{2k}{3}} \tag{39}$$

$$w_{rms} = f_w\zeta\sqrt{\frac{2k}{3}} \tag{40}$$

ζ is a random number drawn from a Gaussian PDF with zero mean and unit variance. Functions f_u, f_v and f_w are given by:

$$f_u = 1 + 0.285(y^+ + 6)\exp[-0.455(y^+ + 6)^{0.53}] \tag{41}$$

$$f_v = 1 - \exp(-0.02y^+) \tag{42}$$

$$f_w = \sqrt{(3 - f_u^2 - f_v^2)} \tag{43}$$

It is pointed out that these functions are valid in the near-wall region where y^+<80 and are Reynolds number dependent.

5.1.5. Dreeben and Pope

Based on the DNS fits of a duct flow (Re = 13000), Dreeben and Pope (1997) proposed to use the following near-wall corrections velocity fluctuations in streamwise, wall-normal and spanwise directions as follows:

$$u^+_{rms} = \frac{\sqrt{\bar{u'^2}}}{u^*} = \frac{0.4y^+}{1 + 0.0239(y^+)^{1.496}} \tag{44}$$

$$v^+_{rms} = \frac{\sqrt{\bar{v'^2}}}{u^*} = \frac{0.116(y^+)^2}{1 + 0.0203(y^+) + 0.0014(y^+)^{2.421}} \tag{45}$$

$$w^+_{rms} = \frac{\sqrt{\bar{w'^2}}}{u^*} = \frac{0.19y^+}{1 + 0.0361(y^+)^{1.322}} \tag{46}$$

It was indicated that these correlations are valid in the near wall region where y^+<100.

5.2. Which near-wall correlation is accurate?

As seen in the previous chapter, several correlations exist for the RMS velocities that can be used to account for the near-wall anisotropy. The not so trivial question is to understand which model is most accurate to be used for RANS modeling. The common factor among all the correlations is the fact that they are derived by fitting a correlation function to the existing experimental and/or DNS data. In order to understand the differences, all the aforementioned correlations are plotted together and compared with the DNS data of Kim et al. (1987).

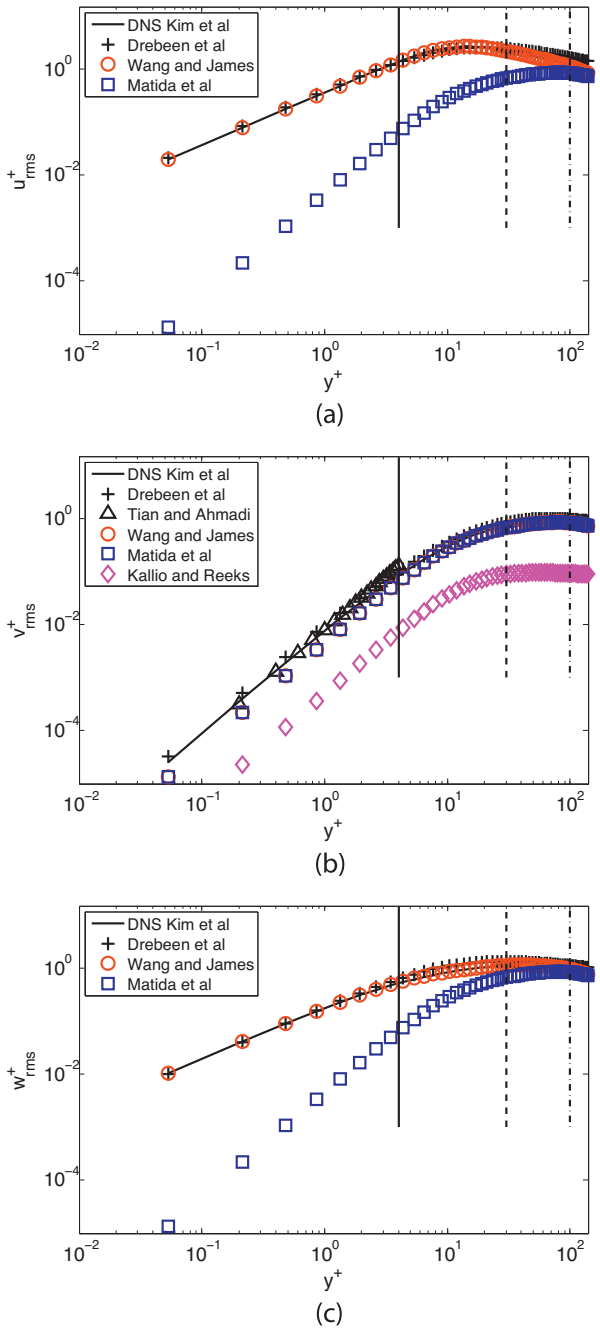

Fig. 2. Comparison of various anisotropic near-wall correlations with the DNS data. (a) Streamwise RMS velocity; (b) Wall-normal RMS velocity; (c) Spanwise RMS velocity.

Fig. 2 shows streamwise, wall-normal and spanwise RMS velocity distributions as a function of non-dimensional wall distance. While the Matida et al. correlation fits the wall-normal RMS velocity well, it severely under-estimates the streamwise and the spanwise RMS velocity. The correlation of Kallio and Reeks for the wall-normal RMS velocity is far from the reference DNS data as this model was essentially derived in the 80's by curve-fitting to the then existing experimental data. All other correlations are consistent when compared to the DNS data. The main outcome of this comparison is:

- Carefully choose a correlation which is accurately representing the DNS data. In the present comparison, both the Drebeen et al.

and the Wang and James correlations are showing good fits to the DNS data. Hence, either of these models can be used.

It should however be noted that these correlations are applicable for fully developed flows since DNS data of fully developed flows are used.

5.3. Is the near-wall DNS data Reynolds number dependent?

It is known that the RMS velocities are slightly dependent on the turbulent Reynolds number (den Toonder and Nieuwstadt, 1997). To investigate how sensitive the near-wall RMS velocities are to the change in Reynolds number, the existing DNS data in the literature are collected and plotted for a wide range of Re_τ. The DNS data are obtained from Kim et al. (1987) and Jimenez and Hoyas (2008). Fig. 3 shows the DNS data of RMS velocities for Re_τ ranging from 180 to 2000. It is observed that all three RMS velocity components are very much similar to each other upto $y^+ \sim 30$. Above y^+ 30, the DNS data starts to show visible Re_τ dependency. The main outcome of this comparison is:

- For y^+<30, the DNS data shows no considerable sensitivity for a range of Re_τ. Hence, near-wall corrections can be applied upto y^+ of 30.

5.4. Is the near-wall DNS data cross-section specific?

Fig. 4 shows streamwise, wall-normal and spanwise RMS velocity distributions as a function of the non-dimensional wall-distance for different flow configurations i.e for a channel and a pipe. The streamwise and the spanwise RMS velocities show very similar profiles for the two different geometries. For the wall-normal RMS velocity, small deviations are observed below y^+ 30. The main outcome of this comparison is:

- The RMS velocity profiles are very similar for the duct flow and the pipe flow configurations at Re_τ 180 and 395.

So far, we have concluded that both Drebeen et al. and the Wang and James correlations are showing good fits to the DNS data. For the present work, we chose to work with the Drebeen et al. correlation. It was also seen that the near-wall correlation can be applied upto y^+ 30 for a wide range of Reynolds numbers. Also, the near-wall correlation showed negligible sensitivity to the varying cross-sectional geometry of a channel flow. Hence, it can be applied for different geometric configurations with fair degree of confidence. Further sensitivity studies are performed by choosing a testcase as described in the next section.

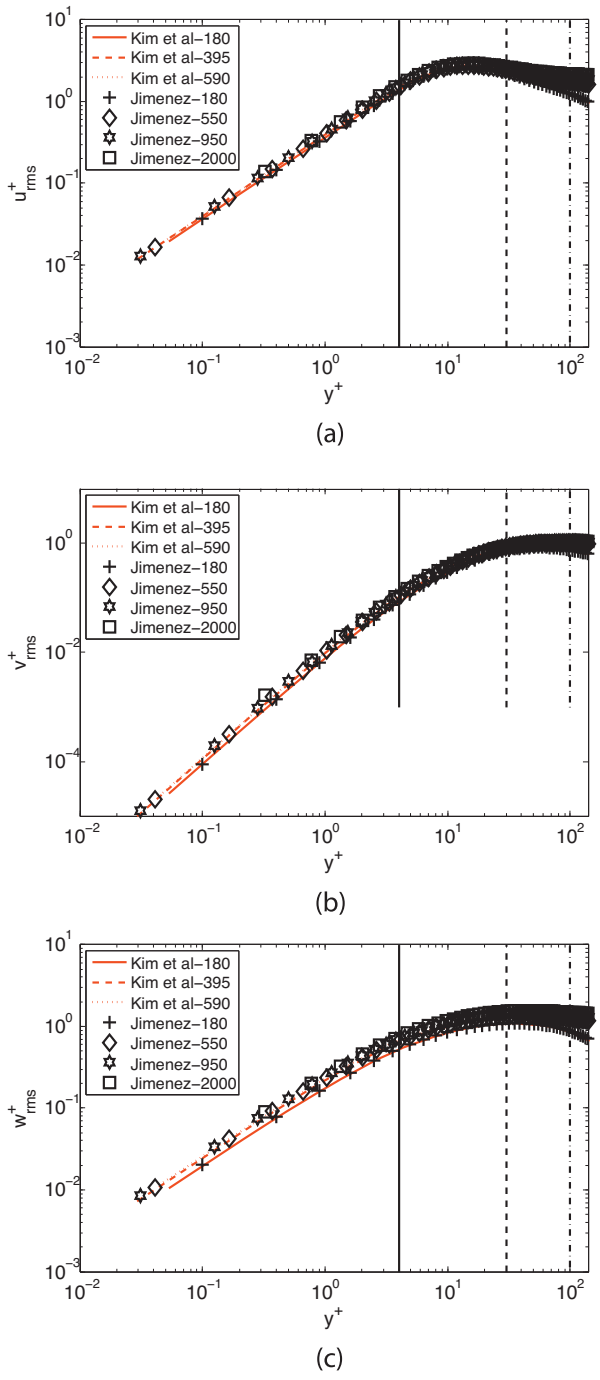

Fig. 3. Comparison of DNS data for various Re_τ. (a) Streamwise RMS velocity; (b) Wall-normal RMS velocity; (c) Spanwise RMS velocity.

6. Testcase

A computational domain considered for the simulation corresponds to a 3D channel with length, width and height of 0.4 m, 0.0628 m and 0.02 m, respectively. A structural hexahedral grid is created with a cell dimension of 0.5 mm in all directions. A higher mesh resolution in the boundary layer is used with the first grid point at a distance of 0.05 mm away from the wall. This corresponds to a non-dimensional wall distance $y^+ = 1$. A growth factor of 1.2 is used, which makes sure that cell sizes grow uniformly from the boundary layer to the bulk. It is worth mentioning that these cell dimensions are also used by Tian and Ahmadi (2007). The total mesh size is about 6 million cells.

The initial air temperature and pressure is assumed to be 288 K and 1 bar. The air density and viscosity is taken to be 1.2 kg/m^3 and 1.84e−05 ns/m^2. The Reynolds number based on the channel width is 6667, which means the flow is turbulent. For the fully developed portion of the duct, the friction velocity u_τ is estimated to be 0.323 m/s. To model turbulence, a standard $k-\varepsilon$ turbulence model with enhanced wall treatment is used. A fully developed profile for velocity, k and ε are applied at the inlet. The values of k and ε are assumed to be zero at the wall while, no-slip boundary condition for velocity is applied. At the outlet, the static atmospheric pressure is assumed. A periodic boundary condition in the spanwise direction is used for the 3D simulation.

The effect of different particle sizes on the deposition velocity are evaluated. For this purpose, different particle sizes ranging from 0.01 μm to 50 μm were considered. The particle density is assumed to be 2400 kg/m^3. The particles are injected at x = 0.2 m where fully

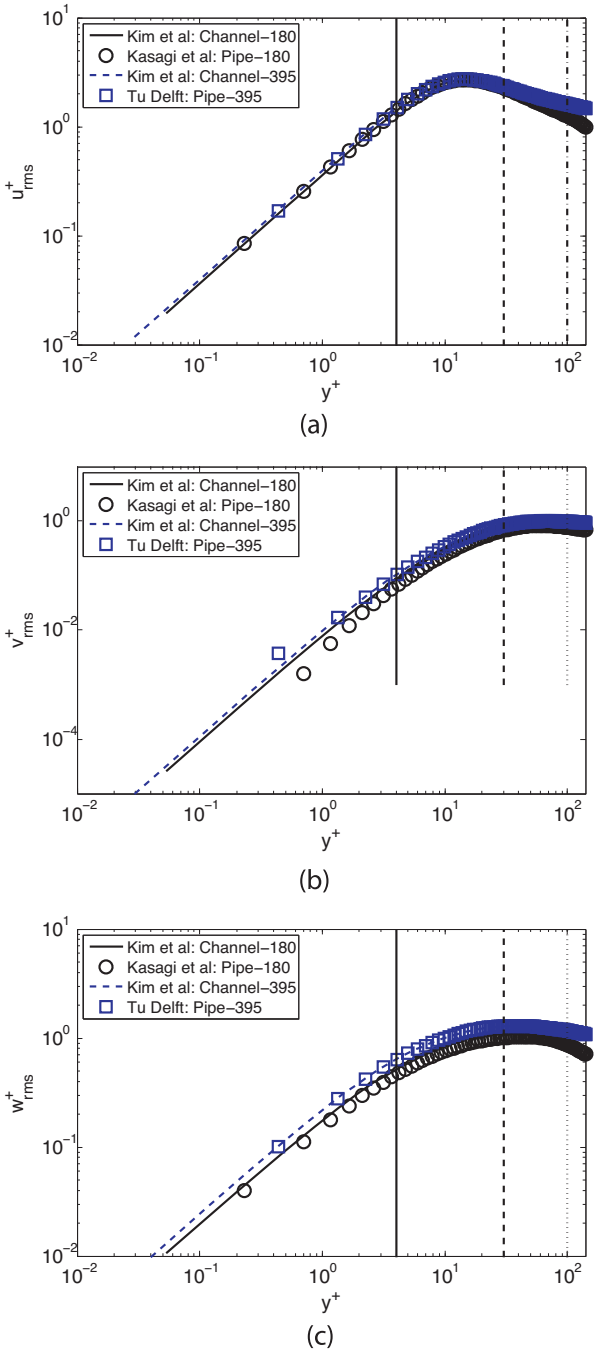

Fig. 4. Comparison of DNS data for channel and pipe flows at Re_τ 180 and 395. (a) Streamwise RMS velocity; (b) Wall-normal RMS velocity; (c) Spanwise RMS velocity.

developed flow is observed. The particles are uniformly distributed at the bottom of the wall, between y^+ 0 and 30. The particles are injected with a velocity equal to the local air velocity. At the inlet and outlet, an "escape" boundary is applied. It implies that the particles leave the computational domain when they touch these boundaries. At the walls, a "trap" boundary condition is imposed. It implies that particles stick to the wall as soon as they come in contact with the wall.

Since the simulation of a 3D channel is expensive for sensitivity studies, as a first step, a simulation is performed to assess whether the computational domain can be represented by a 2D channel. The results of the comparison in Fig. 5 show that the 3D channel can be represented by a 2D channel with no considerable effects on

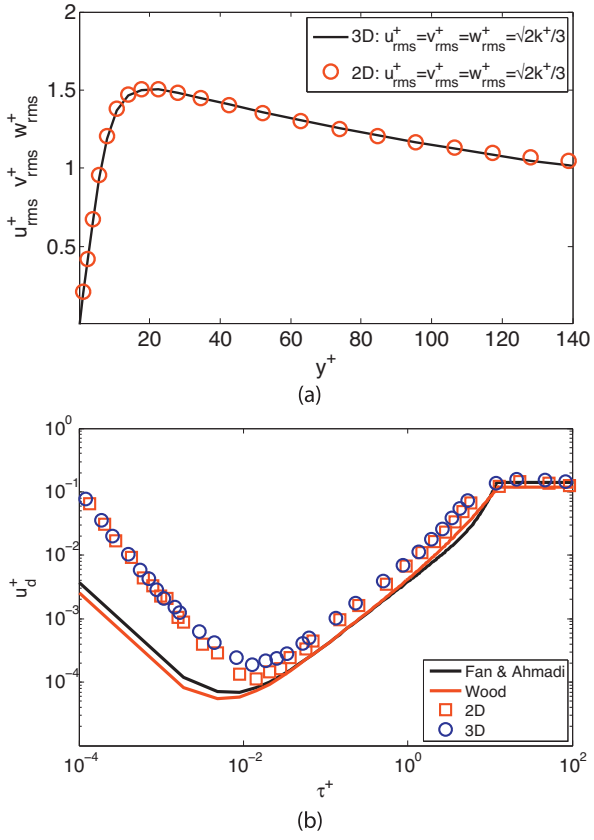

Fig. 5. (a) Comparison of fluid RMS velocity between 3D and 2D channel; (b) Comparison of the non-dimensional deposition velocity between 3D and 2D channel.

the fluid RMS velocity predictions as well as the particle deposition velocity predictions. Hence, for all further sensitivity simulations, a 2D channel is used as the computational domain.

6.1. Postprocessing method

The particle deposition is commonly characterized by non-dimensional deposition velocity:

$$u_d^+ = \frac{J}{C_0 u^*} \tag{47}$$

The deposition velocity is given as a function of the normalized particle relaxation time τ^+. The above expression is valid for particles released with uniform concentration C_0 near a surface. Here, J is the particle mass flux to the wall per unit time. The particle relaxation time is defined as:

$$\tau^+ = \frac{\tau u^{*2}}{\nu} = \frac{S{d_p}^2 u^{*2}}{18\nu^2} C_c \tag{48}$$

where, S is the ratio of particle to fluid density. In the present simulations, the particle deposition velocity is obtained following Tian and Ahmadi (2007) as follows:

$$u_d^+ = \frac{N_d/t_d^+}{N_0/y_0^+} \tag{49}$$

where

$$y_0^+ = \frac{y_0 u^*}{\nu} \tag{50}$$

and

$$t_d^+ = \frac{t_d u*^2}{\nu} \tag{51}$$

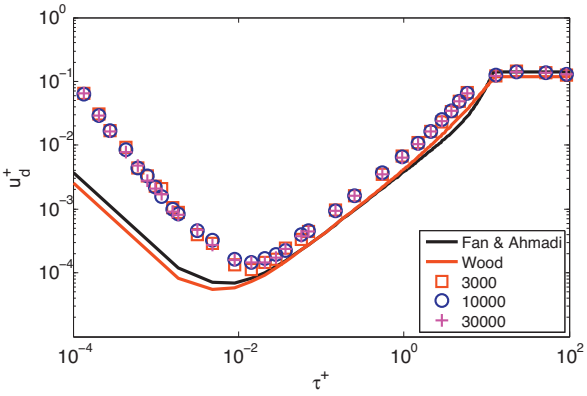

Fig. 6. Comparison of deposition velocity for different number of particle injections.

Here, N_d is the number of deposited particle in the time duration of t_d^+ and N_0 is the initial number of particles uniformly distributed in a region within a distance of y_0^+ from the wall.

A value of 30 for y_0^+ is used, while N_0 is taken to be 3000. These values are recommended by Tian and Ahmadi (2007).

To investigate the influence of the initial number of particles N_0 on the deposition velocity statistics, additional simulations are performed with higher initial numbers of particles. The results in Fig. 6 show that 3000 particles are sufficient to obtain particle number independent results.

7. Numerical aspects

The fluid phase turbulence is modeled using the standard $k-\varepsilon$ model in FLUENT (2011). The spatial discretization of the conservation equations is performed with second-order upwind scheme. The pressure-velocity coupling is performed with the SIMPLE method and discretized equations are solved using a segregated solver in an iterative manner.

For the time integration of the particle motion, there are several numerical schemes available within FLUENT (2011). The performance of the analytic, implicit, trapezoidal and the Runge-kutta scheme are assessed by simulating the horizontal channel. The results in Fig. 7 show that there is no difference between the four available methods. In the present work, the trapezoidal scheme is used for all the simulations.

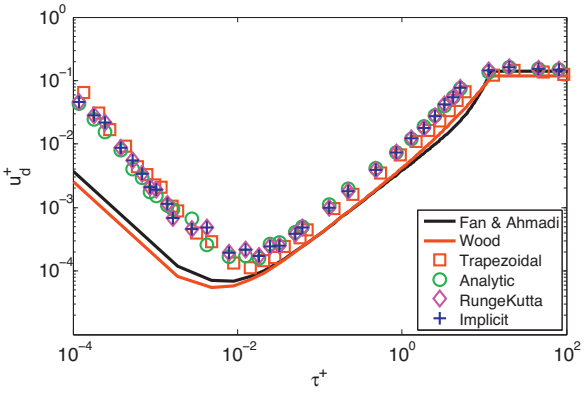

Fig. 7. Performance of different time integration schemes for particle tracking in a 2D channel.

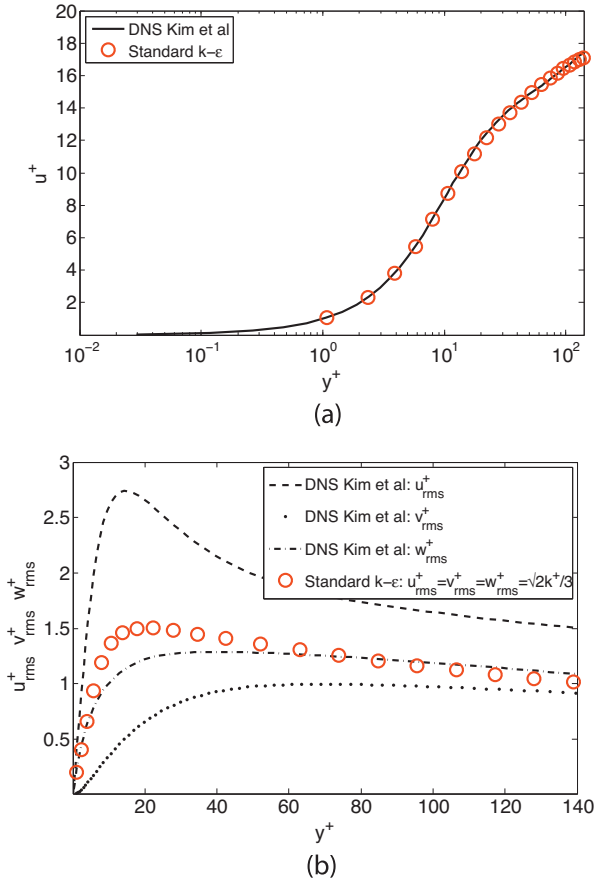

Fig. 8. Comparison of flow predictions by the standard $k-\varepsilon$ model. (Above): Non-dimensional streamwise mean velocity component; (Below): Non-dimensional turbulent kinetic energy.

8. Results

8.1. Fluid phase

The stream-wise mean velocity and the turbulent kinetic energy predictions are shown in Fig. 8. While the mean stream-wise velocity is predicted well in the near-wall region, the turbulent kinetic energy is underestimated. However, if one compares the turbulent kinetic energy to the three fluctuating components of velocity, it is apparent that the kinetic energy in the wall-normal and the spanwise directions are severely over-estimated. This confirms the observation from Tian and Ahmadi (2007) who concluded that isotropic modeling of turbulent kinetic energy in the near-wall leads to unreliable particle deposition predictions.

8.2. Particle phase

8.2.1. Continuous Random Walk or Discrete Random Walk?

DRW approach is presently available in most commerical CFD codes. The recently popular Langevin based CRW model is an attractive alternative model to describe the turbulent fluid fluctuations seen by a particle. The CRW is capable of accurately describing the main features of the turbulent particle dispersion in isothermal inhomogeneous flows as shown in Dehbi (2008a). In order to assess the performance of both CRW and DRW models, RANS simulations of the particle transport and deposition are carried out in a horizontal duct flow. Fig. 9 shows the particle deposition predictions both these approaches. It should be noted that the near-wall anisotropic correction is not applied for the comparison between

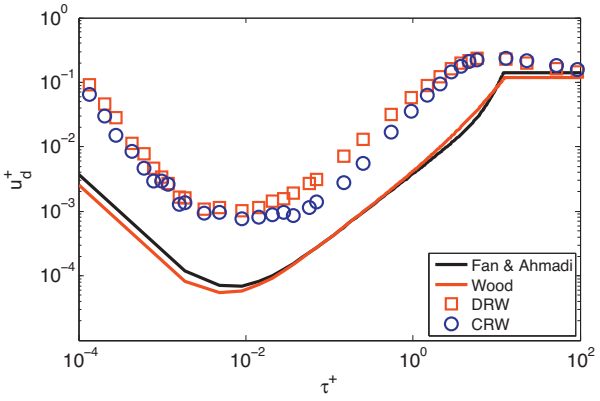

Fig. 9. Comparison of deposition velocity between a CRW approach and a DRW approach.

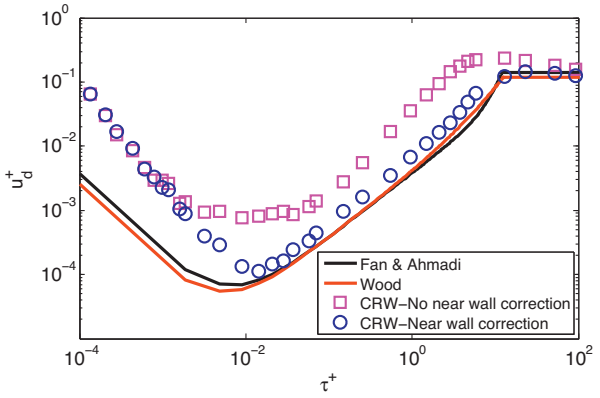

Fig. 10. Comparison of the particle deposition velocity by the isotropic near-wall modeling vs. the anisotropic near-wall modeling.

the CRW and the DRW model. The result shows that there are no distinct differences in the deposition predictions which could prove one model is superior over the other. In the present work, the CRW model is used for all further investigations.

8.2.2. Effect of near-wall correction

As seen before, several correlations exist for the RMS velocities that can be used to account for the near-wall anisotropy. Based on careful evaluation, the correlation of Dreeben and Pope (1997) is chosen for the present work. The importance of taking near-wall anisotropy into account is addressed in this subsection. Fig. 10 shows the comparison of the particle deposition velocity by the isotropic near-wall modeling vs. the anisotropic near-wall modeling. Clearly, accounting for the near-wall anisotropy has resulted in a better match of deposition velocities, especially for the non-dimensional relaxation times between 10^{-2} and 10.

Below 10^{-2}, the results for both the isotropic and the anisotropic models are over-predicted. The particles in this range are predominantly deposited by the Brownian motion. The main reason for the over-prediction is the deficiency in the default Brownian diffusion model available within FLUENT (2011). The work of Inthavong et al. (2009) highlights the deficiency in the default Brownian diffusion model in FLUENT (2011) and recommends an improved model. As Brownian diffusion modeling is out of scope of the present paper, the default model in FLUENT (2011) is retained.

The main outcome of this comparison is:

- Near-wall anisotropy is important and needs to be taken care of in order to obtain realistic deposition velocity predictions.

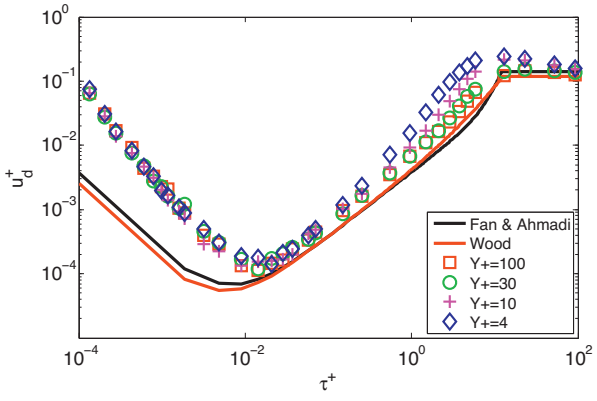

Fig. 11. Particle deposition velocity predictions for different y^+ cut-off values.

8.2.3. Effect of y^+ cutoff

A lot of variability is seen in the literature with respect to the y^+ cut-off value below which the near-wall anisotropy is taken into account. For example, Tian and Ahmadi (2007) propose to use their correlation below y^+=4; Kallio and Reeks (1989) propose to apply their correlation below y^+=200; Wang and James (1999) suggest to use their correlation below y^+=80; Dreeben and Pope (1997) suggest to use their correlation below y^+=100. Considering that all these correlations are basically DNS fits, there is no clear reason for different y^+ cut-off values. Recognizing these differences, it becomes important to test the effect of y^+ cut-off on the deposition predictions. Fig. 11 shows the deposition velocity predictions for various y^+ cut-off values. Most of the sensitivity is observed for the particle relaxation times in range 1 to 10. It is clear that y^+ of 30 and above is required to get a better deposition velocity prediction. Considering that the DNS data in the near-wall region showed Reynolds number dependency after y^+ of 30, it is recommended to use y^+ of 30 as a cut-off. The main outcome of this comparison is:

- A y^+ value of 30 is recommended as a cut-off below which the near-wall anisotropy effects should be considered. Applying anisotropy below y^+ 30 leads to over-estimation of particle deposition velocity in a certain range of particle relaxation times.

8.2.4. Effect of τ_L^+ value in the viscous sub-layer

The Lagrangian integral time scale τ_L^+ appearing in the Langevin equations is used to reproduce the turbulent dispersion of the particle phase. It represents the time over which the velocity of a particle is self correlated. τ_L^+ can generally be rigorously defined for homogeneous turbulence. For inhomogeneous turbulence, it is derived from either the Eulerian spectra of fluctuating velocities or from the Lagrangian calculations by evaluating the Lagrangian autocorrelations. In the present work, we use the fits provided by Kallio and Reeks (1989). For the viscous sub-layer ($y^+ < 5$), a constant value of 10 is recommended for τ_L^+. The Lagrangian DNS simulations of Bocksell and Loth (2006) has estimated the wall normal component of the Lagrangian time scale to be between 2 and 6. Luo et al. (2007) have worked out an average value of the wall normal Lagrangian time scale to be between 3 and 5. Since a range of τ_L^+ are reported in the literature, the effect of it on the particle deposition velocity is tested. Fig. 12 shows the deposition velocity predictions for τ_L^+ values of 2, 6 and 10. As seen, there is no considerable influence of this constant on the deposition velocity predictions. The main outcome of this comparison is:

- The values of 2, 6 and 10 for τ_L^+ in the region below y^+ of 5 have no considerable effect on the deposition velocity predictions.

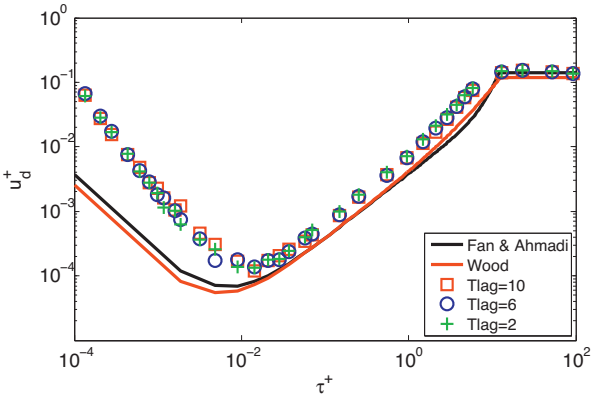

Fig. 12. Particle deposition velocity predictions for different τ_L^+ cut-off values.

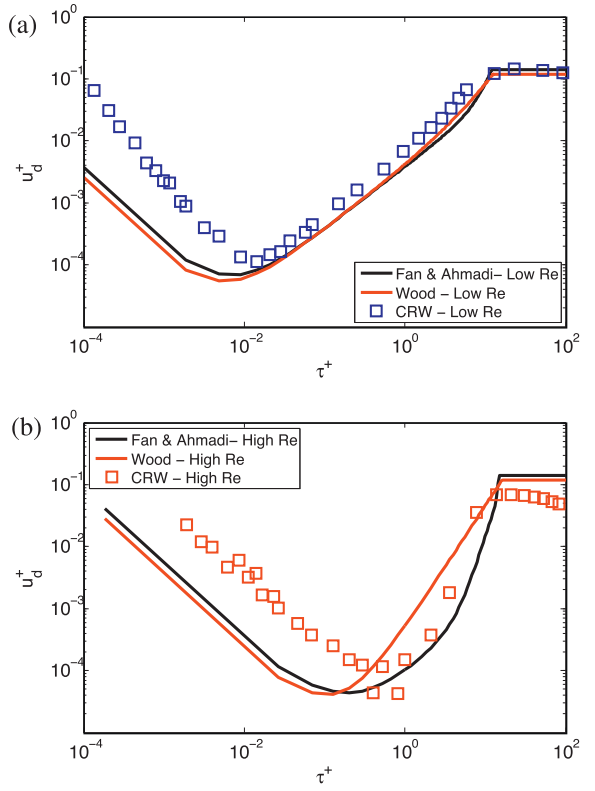

Fig. 13. Particle deposition velocity predictions at different Reynolds numbers.

8.2.5. Effect of Reynolds number

It has been shown that the near-wall DNS statistics up to y^+ 30 are relatively universal for a wide range of Re_τ. The simulations so far were performed at a Reynolds number of 6667. In order to verify if one can apply the near-wall correlations at different Reynolds numbers, a duct flow simulation at 5 times higher Reynolds number is performed. With increase in Reynolds number, the effect of particle resuspension becomes important. This is especially true when the friction velocity u_τ bocomes greater than 0.3 m/s in a channel flow (Barth et al., 2014; Lecrivain et al., 2014). However, the particle resuspension is out of scope of the present article's objectives and hence not considered.

Fig. 13 shows the deposition velocity predictions at two different Reynolds numbers. It is seen that the deposition velocity predictions at a higher Reynolds number are also consistent with the comparison data. The main outcome of this comparison is:

- The present near-wall correlations can be applied to a wide range of Reynolds numbers.

9. Conclusions

Several uncertainties relating to the near-wall modeling of particle transport and deposition are addressed for the RANS approach. The main conclusions drawn from the validation analyses performed in a fully developed duct flow are as follows:

- Several correlations exist in the literature to model the near-wall anisotropy in the fluid phase. Carefully choose a correlation which is accurately representing the DNS data. In the present work, both the Drebeen et al. and the Wang and James correlations are showing good fits to the DNS data. Hence, either of these models can be used.
- For y^+<30, the DNS data showed no considerable sensitivity for a range of Re_τ. Hence, near-wall corrections can be applied up to y^+ of 30.
- The RMS velocity profiles are very similar for the duct flow and the pipe flow configurations at Re_τ 180 and 395 implying negligible sensitivity to changing cross-section.
- From the fluid flow results, it is apparent that the kinetic energy in the wall-normal and the spanwise directions is severely overestimated. Hence, there is the need for anisotropic correlations close to the wall.
- There were no considerable differences in the particle deposition patterns predicted by the CRW model and the DRW model.
- Particle deposition predictions show that the near-wall anisotropy is important and needs to be taken care of in order to obtain realistic deposition velocity predictions.
- A y^+ value of 30 is recommended as a cut-off below which the near-wall anisotropy effects should be considered. Applying anisotropy below y^+ 30 leads to over-estimation of particle deposition velocity in a certain range of particle relaxation times.
- The values of 2, 6 and 10 for τ_L^+ in the region below y^+ of 5 have no considerable effect on the deposition velocity predictions.
- The present near-wall correlations can be applied to a wide range of Reynolds numbers.

Future work

The conclusions drawn in the present paper are specifically based on the validation analyses performed in a fully developed duct flow. This is the first step towards the validation analysis. The presently validated models in a duct flow should be tested on more complex flow configurations such as the bend pipe flow, flow around single spheres, flow around array of spheres, flow around symmetric pebble-beds and eventually flow over random pebble beds. This work is currently in progress and will form a part of the follow-up paper.

Acknowledgement

The work described in this paper is funded by the Dutch Ministry of Economic Affairs, the FP7 EC Collaborative Project THINS No. 249337, and the FP7 EC Collaborative Project ARCHER No. 269892.

References

Agnihotri, V., Ghorbaniasl, G., Verbanck, S., Lacor, C., 2012. An Eddy interaction model for particle deposition. J. Aerosol Sci. 47, 39–47.
Barth, T., Preu, J., Mller, G., Hampel, U., 2014. Single particle resuspension experiments in turbulent channel flows. J. Aerosol Sci. 71 (0), 40–51.
Bockell, T.L., Loth, E., 2006. Stochastic modeling of particle diffusion in a turbulent boundary layer. Int. J. Multiph. Flow 32, 1234–1253.

Bocksell, T., Loth, E., 2006. Stochastic modeling of particle diffusion in a turbulent boundary layer. Int. J. Multiph. Flow 32, 1234–1253.
CEA, 2006. Gas-cooled nuclear reactors: A monograph of the nuclear energy directorate. CEA Saclay et Groupe Moniteur, ISBN 2-281-11343-4.
Crowe, C., Sommerfeld, M., Tsuji, Y., 1998. Multiphase Flows with Droplets and Particles. CRC Press, Boca Raton.
Dehbi, A., 2008a. A CFD model for particle dispersion in turbulent boundary layer flows. Nucl. Eng. Des. 238, 707–715.
Dehbi, A., 2008b. Turbulent particle dispersion in arbitrary wall-bounded geometries: a coupled CFD-Langevin-equation based approach. Int. J. Multiph. Flow 34 (9), 819–828.
Dehbi, A., 2009. A stochastic Langevin model of turbulent particle dispersion in the presence of thermophoresis. Int. J. Multiph. Flow 35 (3), 219–226.
Dehbi, A., 2010. Validation against dns statistics of the normalized langevin model for particle transport in turbulent channel flows. Powder Technol. 200 (1-2), 60–68.
Dehbi, A., de Crcy, F., 2011. Validation of the Langevin particle dispersion model against experiments on turbulent mixing in a T-junction. Powder Technol. 206 (3), 312–321.
den Toonder, J.M.J., Nieuwstadt, F.T.M., 1997. Reynolds number effects in a turbulent pipe flow for low to moderate re. Phys. Fluids 9 (11).
Dreeben, T.D., Pope, S.B., 1997. Probability density function and Reynolds-stress modeling of near-wall turbulent flows. Phys. Fluids 9, 154–163.
FLUENT, 2011. Fluent user's guide 14.0.
Gosman, A., Ioannides, E., 1983. Aspects of computer simulation of liquid-fuelled combustors. J. Energy 7, 482–490.
Gosman, A.D., Ioannides, E., 1981. Aspects of computer simulation of liquid-fuelled combustor. AIAA J., 81–0323.
Gottaut, H., Kruger, H., 1990. Results of experiments at the AVR reactor. Nucl. Eng. Des. 121, 143–153.
He, C., Ahmadi, G., 1999. Particle deposition in a nearly developed turbulent duct flow with electrophoresis. J. Aerosol Sci. 30 (6), 739–758.
Hutchinson, P., Hewitt, G.F., Dukler, A.E., 1971. Deposition of liquid or solid dispersions from turbulent gas streams: a stochastic model. Chem. Eng. Sci. 26, 419–439.
Inthavong, K., Zhang, K., Tu, J., 2009. Modeling submicron and micron particle deposition in a human nasal cavity. In: Seventh International Conference on CFD in the Minerals and Process Industries.
Jimenez, J., Hoyas, S., 2008. Turbulent fluctuatations above the buffer layer of wall-bounded flows. J. Fluid Mech. 611, pages 215-236. 611, 215-236.
Kallio, G.A., Reeks, M.W., 1989. A numerical simulation of particle deposition in turbulent boundary layers. Int. J. Multiph. Flow 15-3, 433–446.
Kim, J., Moin, P., Moser, R.D., 1987. Turbulent statistics in fully developed channel flow at low reynolds number. J. Fluid Mech. 177, 133–166.
Kissane, M.P., 2009. A review of radionuclide behaviour in the primary system of a vhtr. Nucl. Eng. Des. 239, 3076–3091.
Kissane, M.P., Zhang, F., Reeks, M.W., 2011. Dust in HTRS: its nature and improving prediction of its resuspension. Nucl. Eng. Des., http://dx.doi.org/10.1016/j.nucengdes.2011.10.028
Lai, A., Chen, F., 2006. Modeling particle deposition and distribution in a chamber with a two-equation Reynolds-averaged Navier–Stokes model. Aerosol Sci. 37, 1770–1780.
Lecrivain, G., Hampel, U., 2012. Influence of the Lagrangian integral time scale estimation in the near wall region on particle deposition. J. Fluids Eng. 134 (7).
Lecrivain, G., Sevan, D.M., Tomas, B., Hampel, U., 2014. Numerical simulation of multilayer deposition in an obstructed channel flow. Adv. Powder Technol. 25, 310–320.
Li, A., Ahmadi, G., 1992. Dispersion and deposition of spherical particles from point sources in a turbulent channel flow. Aerosol Sci. Technol. 16, 209–226.
Liu, B.Y.H., Agarwal, J.K., 1974. Experimental observation of aerosol deposition in turbulent flow. J. Aerosol Sci. 5-2, 145–158.
Luo, J., Ushijima, T., Kitoh, O., Lu, Z., Liu, Y., 2007. Lagrangian dispersion in turbulent channel flow and its relationship to eulerian statistics. Int. J. Heat Fluid Flow 28 (5), 871–881.
Luo, X.W., Yu, S.Y., Zhang, Z.S., He, S.Y., 2005. Estimation of graphite dust quantity and size distribution of graphite particle in HTR-10. Nucl. Power Eng. 26 (2), 203–208.
Maciines, J., Bracco, F., 1992. Stochastic particle dispersion modeling and the tracer particle limit. Phys. Fluids A 4, 2809–2823.
Macinnes, J.M., Bracco, F.V., 1992. Stochastic particle dispersion modeling and the tracer-particle limit. Phys. Fluids 4, 2809–2824.
Mansour, N., Kim, J., Moin, P., 1988. Reynolds-stress and dissipation-rate budgets in a turbulent channel flow. J. Fluid Mech. 194, 15–44.
Marchioli, C., Soldati, A., Kuerten, J.G.M., Arcen, B., Taniere, A., Goldensoph, G., Squires, K.D., Cargnelutti, M.F., Portela, L.M., 2008. Statistics of particle dispersion in DNS of wall-bounded turbulence: results of an international collaborative benchmark test. Int. J. Multiph. Flow 34, 879–893.
Matida, E.A., Finlay, W.H., Lange, C.F., Grgic, B., 2004. Improved numerical simulation of aerosol deposition in an idealized mouth-throat. J. Aerosol Sci. 35, 1–19.
Mito, Y., Hanratty, T., 2002. Use of a modified Langevin equation to describe turbulent dispersion of fluid particles in a channel flow. Flow Turbul. Combust. 68, 1–26.
Mito, Y., Hanratty, T., 2004. A stochastic description of wall sources in a turbulent field. part 2. calculation for a simplified model of horizontal annular flows. Int. J. Multiph. Flow 30, 803–825.
Ounis, H., Ahmadi, G., McLaughlin, J., 1993. Brownian particle deposition in a directly simulated turbulent channel flow. Phys. Fluids A 5, 1427–1432.
Sommerfeld, M., Ando, A., Wennerberg, D., 1992. Swirling, particle-laden flows through a pipe expansion. ASME: J. Fluids Eng. 114, 648–656.
Tian, L., Ahmadi, G., 2007. Particle deposition in turbulent duct flows – comparison of different model predictions. J. Aerosol Sci. 38, 377–397.
Wang, Y., James, P.W., 1999. On the effect of anisotropy on the turbulent dispersion and deposition of small particles. Int. J. Multiph. Flow 25, 551–558.